The 15th International Symposium on Magnetic Bearings, August 3-6, 2016, Mojiko Hotel, Kitakyushu, Japan

ISMB15

Influence of Unbalance Levels on Nonlinear Dynamics of a Rotor-Backup Rolling Bearing System

Cesar FONSECA*, Ilmar SANTOS* and Hans WEBER**

* Dept. of Mechanical Engineering, DTU
Niels Koeppel Allé, 404, 2800, Lyngby, Denmark
E-mail: cefonse@dtu.mek.dk

** Dept. of Mechanical Eng., PUC-Rio
Rua Marquês de de São Vicente, 225, 22451-900, Rio de Janeiro, Brazil

Abstract

Rotor drops in magnetic bearing and unbalance in rotors have been objective of study for many years. The combination of these two well-known phenomena led to an interesting chaotic response, when the rotor touches the inner race of the back-up bearing. The present work explores the nonlinear rotor-backup-bearing dynamics both theoretically and experimentally using a fully instrumented test rig, where the position of shaft, its angular velocity and the contact forces between the shaft and the backup bearing are sampled at 25 kHz. The test rig is built by a removable passive magnetic bearing, which allows for simulation of magnetic bearing failure (loose of carrying capacity and rotor fall). A theoretical approach is given beforehand and supplies the basis of the study. Finally the presented results are commented on the point of view of nonlinear dynamics applied to the practical use. The theoretical and numerical analyzes are shown through Poincaré maps and double sided spectrum. The latter is important to characterize the condition at different levels of unbalance between forward of backwards whirl. Our preliminary results indicate that for small levels of unbalance the rotor oscillates at the bottom of the backup bearing. When the levels of unbalance increase, the dynamical behaviour of the rotor changes, leading to extremely harmful conditions, since the rotor can be lifted from the bottom of the bearing (contact state) and return, starting to impact on the backup inner race innumerable times without reaching a steady state.

Key words : Safety bearings, impact, friction, contact mechanics, nonlinear dynamics, magnetic bearing.

1. Introduction

The possibility to use magnetic bearing rotor in industrial applications cannot be thought correctly without the use of proper back-up bearings. Applications are many such as reaction wheels, centrifuges, energy efficiency machines, (Gasch et al., 2002), (Schweitzer and Maslen, 2009), and among others. For all these machines, a safety element has to be installed to prevent failures such as, power loss, that would cause the shaft to fall. The safety element consists normally of a rolling bearing with inner race diameter bigger than the shaft diameter, but smaller than the one at the magnetic bearing. It is designed to withstand the loads and impacts of a rotor. It also protects the whole system and prevents even more disastrous situations.

Throughout the years, several works have been published on this subject. (Muszynska, 1989) has given a good overview of the state of rotordynamics research of rub-related phenomena. In the work of (Johnson, 1962) a vertical shaft with clearance with impacts was studied . (Black, 1968) published a work of a two-degree-of-freedom rotor and stator, which is highly cited through the years. While in (Wojciech, M. S., 1986), a gyro pendulum with a piecewise linear model was investigated with a good agreement with experimental results. (Zhang, 1988) showed a multi-degree model rotor at a full annular rub using Black's model. (Choy and Padovan, 1987) showed also the interaction between the rotor and the casing on a bearing wall. By employing a proper impact model, chaos was reported by (Goldman and Muszynska, 1994). (Piccoli and Weber, 1998) investigated an application to identify chaotic motion with Lyapunov exponents and Poincaré Diagrams. In (Jiang and Ulbrich, 2005), dry friction whip investigated with an unbalanced rotor to stator contact. One of the most cited is the work from (Pradetto and Schmied, 1992), where a one-ton rotor drop is analyzed. (Fumagalli, 1997) tested the performance of a rotor sliding and tumbling while touching the auxiliary bearing.

In combination with Active Magnetic Bearings (AMB) technology, (Schweitzer, 1975), it is clear that safety bearings

are an important subject of study. (Kirk, 1996) analyzed numerically the transient response of a rotor drop. (Ginzinger et al., 2009) developed an active actuator to avoid severity of the contact. Moreover, in (Keogh, 2012), a comprehensive study of different performance on auxiliary bearings was presented. Non-conventional geometries of the back-up bearing were considered by (Simon, 2001), and later by (Zülow and Liebich, 2009) and then the new kind of bearing with pins is presented by (Lahriri and Santos, 2012) and analyzes the forces that the structure receives, where the backup is. In (Fonseca et al., 2015) it is shown that the same pins help to surpass the critical speed avoiding the backwards whirl. However, in most industrial operating machines, the safety bearing is a common rolling bearing element, and the rotor will lay down at the bottom allowing it to rotate without much damage to the system. An analysis of the rigid rotor on a safety bearing showing chaotic behavior is shown by (Wang and Noah, 1998). Later the contact between the shaft and the inner race was modeled using a finite element and was presented by (Cole et al., 2001). More recently, (Inayat-Hussain, 2010) gives an insight about the response of the rotors to different parameters with the bifurcation diagrams.

In this work, a theoretical and an experimental study of a passive magnetic bearing rotor colliding on the ball bearing inner race is presented. The failure of the rotor will be induced by the rapid removal of the passive magnetic bearing letting the rotor to fall. The tests will be compared with simulated results coming from a model of the rotor as a rigid body impacting on an compliant surface. The main contribution of this work is to show that different levels of unbalance change the dynamical behavior of the system and may lead to harmful situations, for which the backup bearing is not designed.

2. Modeling the rotor-housing kinematics

2.1. The shaft

In Figure 1a and b, the mathematical model of the rotor is built to reproduce the assembled test rig. The rotor is supported by one spherical ball bearing at point 0 and one movable passive magnetic bearing at point C. The back-up bearing is mounted between them at point B. The rotor is modeled as a rigid body and external forces from the magnets, imbalance and coupling are applied at points C, A and D respectively. The rotor is only allowed to rotate according to the following three angular degrees of freedom: $\Gamma(t)$, $\beta(t)$, $\theta(t)$ and the angular velocities:

$$ {}_I\dot{\Gamma} = \begin{bmatrix} \dot{\Gamma}(t) & 0 & 0 \end{bmatrix}^T, \quad {}_{B1}\dot{\beta} = \begin{bmatrix} 0 & \dot{\beta}(t) & 0 \end{bmatrix}^T \text{ and } \quad {}_{B2}\dot{\theta} = \begin{bmatrix} 0 & 0 & \dot{\theta}(t) \end{bmatrix}^T. \tag{1} $$

In figure 1a it is possible to see the reference frames used and the moving reference frame, $B3$, fixed to the rotating shaft and positioned at the supporting point of the rotor.

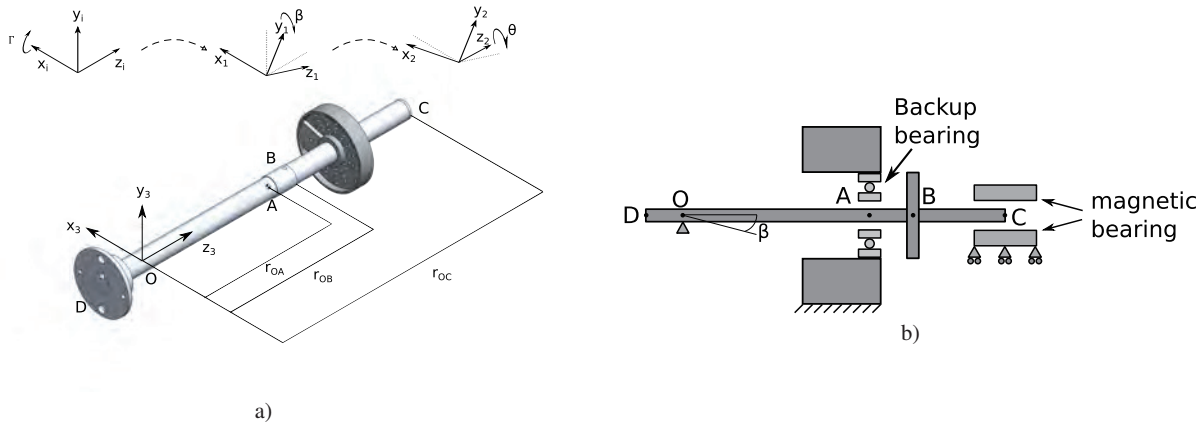

Fig. 1 The moving frame references and the points of interests, A, B and C, where forces are present.

$$ {}_I T_\Gamma = \begin{bmatrix} 1 & 0 & 0 \\ 0 & \cos\Gamma(t) & \sin\Gamma(t) \\ 0 & -\sin\Gamma(t) & \cos\Gamma(t) \end{bmatrix}, \quad {}_{B1}T_\beta = \begin{bmatrix} \cos\beta(t) & 0 & -\sin\beta(t) \\ 0 & 1 & 0 \\ \sin\beta(t) & 0 & \cos\beta(t) \end{bmatrix}, \quad {}_{B2}T_\theta = \begin{bmatrix} \cos\theta(t) & \sin\theta(t) & 0 \\ -\sin\theta(t) & \cos\theta(t) & 0 \\ 0 & 0 & 1 \end{bmatrix}. \tag{2} $$

Each external force will generate a moment with respect to O and the relevant position vector are given by:

$$ {}_{B3}r_{OA} = \begin{bmatrix} r_{OA,x} & 0 & r_{OA,z} \end{bmatrix}^T, \quad {}_{B3}r_{OB} = \begin{bmatrix} r_{OB,x} & r_{OB,y} & r_{OB,z} \end{bmatrix}^T \quad \text{and} \quad {}_{B3}r_{OC} = \begin{bmatrix} 0 & 0 & r_{OC,z} \end{bmatrix}^T. \tag{3} $$

The inertia tensor referred to the supporting point is:

$$ {}_{B3}I_O = \begin{bmatrix} I_{xx} & 0 & -I_{xz} \\ 0 & I_{yy} & 0 \\ -I_{zx} & 0 & I_{zz} \end{bmatrix}. \tag{4} $$

where $I_{xz} = m_u r_u l_{OD}$. The absolute angular velocity of the represented at the moving reference frame B3 (where the inertia tensor is constant) is given by:

$$ \omega_{B3} = {}_{B3}\dot{\Gamma} + {}_{B3}\dot{\beta} + {}_{B3}\dot{\theta} = \begin{bmatrix} \cos(\theta)\cos(\beta)\dot{\Gamma} + \sin(\theta)\dot{\beta} \\ -\sin(\theta)\cos(\beta)\dot{\Gamma} + \cos(\theta)\dot{\beta} \\ \sin(\beta)\dot{\Gamma} + \dot{\theta} \end{bmatrix}. \tag{5} $$

The absolute acceleration is given by:

$$ \dot{\omega}_{B3} = \begin{bmatrix} -\dot{\theta}\sin(\theta)\cos(\beta)\dot{\Gamma} - \cos(\theta)\dot{\beta}\sin(\beta)\dot{\Gamma} + \cos(\theta)\cos(\beta)\ddot{\Gamma} + \dot{\theta}\cos(\theta)\dot{\beta} + \sin(\theta)\ddot{\beta} \\ -\dot{\theta}\cos(\theta)\cos(\beta)\dot{\Gamma} + \sin(\theta)\dot{\beta}\sin(\beta)\dot{\Gamma} - \sin(\theta)\cos(\beta)\ddot{\Gamma} - \dot{\theta}\sin(\theta)\dot{\beta} + \cos(\theta)\ddot{\beta} \\ \dot{\beta}\cos(\beta)\dot{\Gamma} + \sin(\beta)\ddot{\Gamma} + \ddot{\theta} \end{bmatrix}. \tag{6} $$

2.2. The inner and outer housing

In order to determine and acquire the force between the rotor shaft and the inner race, the back-up bearing is mounted on an special casing, where there are four force transducers. The elastic elements k_{ft} represent the force transducers positioned between the bodies and the damping elements, c_h and c_v are structural damping. These damping terms are present due to the four beams that hold the inner house to slide vertically and the outer house horizontally, two for each directions. The back-up bearing is inside a block that is mounted inside a frame, called outer house. Then, the inner house is only allowed to move horizontally inside it. Subsequently, the outer house moves only vertically. Figure 2a and Figure 2b show a schematic of the complete assembly.

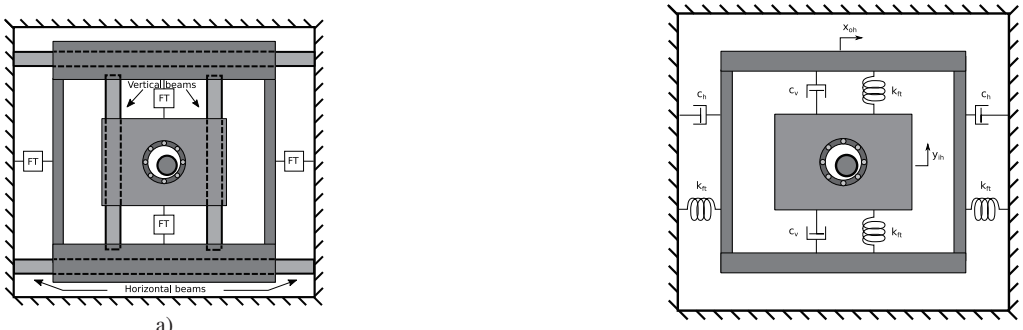

Fig. 2 Assembly of the inner housing and the outer housing.

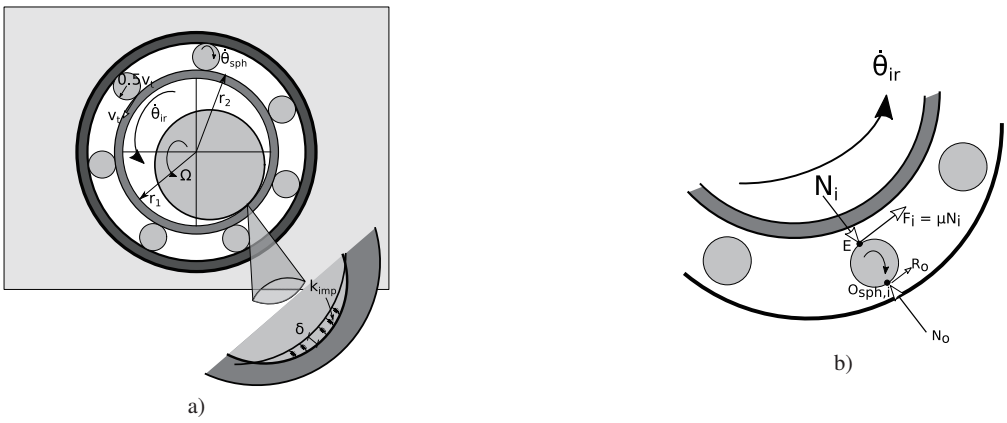

Fig. 3 Left: The shaft inside the inner bearing. Right: The forces acting at each ball of the back-up bearing.

The dynamics of both housings are included in the mechanical model. The dynamic coupling between the inner house and the rotor is introduced by the impact forces, N and the friction force F_{fric}. The beams that support the housings have the stiffness calculated as clamped-clampled beam $K_{beam} = \frac{48EI}{Fa^2(3l-4a)}$. and the damping coefficients approximated by:

$$c_h = 2\zeta\sqrt{K_{beam}\,(m_{ih} + m_{oh})} \quad \text{and} \quad \mathrm{c_v} = 2\zeta\sqrt{K_{beam}\,(m_{ih})}. \tag{7}$$

Thus the governing equations of both housings are written in Equations (8) and (9)

$$m_{ih}\ddot{y}_{ih} = -2k_{ft}y_{ih} - 2c_v y_{ih} - m_{ih}g + N\sin\alpha + F_{fric}\cos\alpha. \tag{8}$$

$$(M_{oh} + m_{ih})\,\ddot{x}_{oh} = -2k_{ft}x_{oh} - 2c_h x_{oh} + N\cos\alpha - F_{fric}\sin\alpha. \tag{9}$$

Consequently, the radial term r_r can be calculated and allows one to know whether the system is impacting or not, and it is equal to:

$$r_r = \sqrt{(\beta l_{OB} - x_{oh})^2 + (-\Gamma l_{OB}) - y_{ih})^2}. \tag{10}$$

The impact is analysed at each time step if the rotor displacement at the position of the back-up bearing is bigger or equal than the radial gap, $\delta \geq r_0 = r_1 - r_r$. The impact is modeled following a stepwise elastic model proposed by (Lankarani and Nikravesh, 1990):

$$F_{imp} = N = k_{imp}\delta^{3/2}\left(1 + \frac{3(1-e^2)}{4}\frac{\dot{\delta}}{\dot{\delta}^-}\right), \quad \text{if} \quad \delta \geq 0, \tag{11}$$

in which the stiffness coefficient is given as:

$$k_{imp} = \frac{4}{3\left(\frac{1-\nu_s^2}{E_s} + \frac{1-\nu_i^2}{E_i}\right)}\left(\frac{r_s r_1}{r_1 - r_s}\right)^{1/2}. \tag{12}$$

Therefore, the forces acting on the mechanical model are the rotor's own weight, the magnetic force and the damping force plus the impact forces

$${}_I\mathbf{F}_g = \begin{bmatrix} 0 \\ -mg \\ 0 \end{bmatrix},\ {}_I\mathbf{F}_{mag} = \begin{bmatrix} -K\cos\alpha \\ -K\sin\alpha \\ 0 \end{bmatrix},\ {}_I\mathbf{F}_{damp} = \begin{bmatrix} -c\cos\rho \\ -c\sin\rho \\ 0 \end{bmatrix},\ {}_I\mathbf{F}_{imp} = \begin{bmatrix} N\cos\alpha \\ N\sin\alpha \\ 0 \end{bmatrix} \text{ and } {}_I\mathbf{F}_{fric} = \begin{bmatrix} F_{fric}\sin\alpha \\ F_{imp}\cos\alpha \\ 0 \end{bmatrix}. \tag{13}$$

Finally one writes Euler's equation with respect to the supporting point O

$$\sum {}_{B3}\text{Force Moments}_O = {}_{B3}\,I_O\left(\frac{\mathrm{d}}{\mathrm{dt}}\omega_{B3}\right) + {}_{B3}\,\omega \times ({}_{B3}I_O \cdot {}_{B3}\,\omega) \tag{14}$$

and solves the set of equation considering the angles Γ and β small. The motor has an independent control and is capable to deliver the necessary torque to keep the angular velocity to $\dot{\theta}$. The differential equations are highly nonlinear with many coupled terms and the solution is found using the symbolic program Maple®. However, we are more interested in the position of the center of shaft at the backup bearing plane and using the transformation matrices, the coordinates are written as:

$$\begin{bmatrix} X \\ Y \\ Z \end{bmatrix} = \left({}_I T_\Gamma^T(t) \cdot {}_{B1}\,T_\beta^T(t) - {}_I T_\Gamma^T(0) \cdot {}_{B1}\,T_\beta^T(0)\right) \cdot {}_{B2}\,r_{OC}, \tag{15}$$

where the initial conditions are taken into consideration, $t = 0$, $\Gamma(0) = 0$ and $\beta(0) = 0$.

2.3. The back-up bearing

When the rotor falls and hits the rolling back-up bearing, Figure 3, the friction force accelerates the inner race and the spheres.The angular position of the inner race, θ_{Ir}, is also a degree of freedom. Figure 3a illustrates a schematic view of balls and inner race and their velocities. Since the outer race is not moving and the spheres are not sliding on the touching point with it, point O_{sph}, the tangential velocity is half of the one on the edge between the sphere and the inner

race, point E. The force acting on one rolling bearing ball is shown in Figure 3b the following equations for one isolated ball are written in (16)-(18):

$$\sum \text{Moment}_{O_{sph}} = I_{sph}\ddot{\theta}_{sph} \tag{16}$$

$$2r_{sph}F_i = I_{sph}\ddot{\theta}_{sph}, \quad \text{since, } v_t = \dot{\theta}_{ir}r_2 = \dot{\theta}_{sph}r_{sph}, \tag{17}$$

$$2r_{sph}F_i = I_{sph}\ddot{\theta}_{ir}\frac{r_2}{r_{sph}}, \tag{18}$$

where $I_{sph} = 2/5\left(\pi r_{sph}^2\right) + m_{sph}r_{sph}^2$. Newton equation for the tangential direction leads to:

$$F_i + R_o = m_{sph}a_t. \quad \text{From (17) and (18), } R_o + I_{sph}\ddot{\theta}_{ir}\frac{r_2}{2\left(r_{sph}\right)^2} = m_{sph}\ddot{\theta}_{ir}r_2. \tag{19}$$

Therefore the angular acceleration of the inner race, $\ddot{\theta}_{ir}$ can be obtained taking into account the influence of all rolling spheres j.

$$\ddot{\theta}_{ir}I_{ir} = fr_1 - r_2\sum_{j=1}^{N_{sph}}\left(F_{i,j}\right), \tag{20}$$

$$\ddot{\theta}_{ir}I_{ir} = fr_1 - r_2N_{sph}\left(\ddot{\theta}_{ir}\frac{I_{sph}r_2}{2\left(r_{sph}\right)^2}\right) \rightarrow \ddot{\theta}_{ir}\left(I_{ir} + N_{sph}\frac{I_{sph}}{2}\left(\frac{r_2}{r_{sph}}\right)^2\right) = fr_1. \tag{21}$$

3. Simulation and nonlinear analysis

3.1. Integration in time

The governing equations (14), (20), (8), and (9) are integrated in time using a combined Matlab differential equation solver *ode45* and a dedicated Runge-Kutta algorithm. The former is employed together with an *Event* function in order to find the exact moment of the impact. The latter is applied during the short period of impact. It was done so, because it is a highly stiff problem and demands an enormous time with very tight integration tolerances of the algorithm. Therefore a test of convergence was performed and the adequate step time was set to 10^{-6} s. During the impact the relative velocity between the shaft and the inner race, v_{rel}, plays an important role. The friction force is dependent on it. If the velocities match, there is no friction. Otherwise, the friction force is modeled as $F = \mu N\text{sign}\left(v_{rel}\right)$. The model parameters are shown in table 1.

Table 1 Parameters set applied to the simulation.

Parameter of the shaft	
Mass without unbalance	$m = 1.28$ kg
Length to magnetic bearing	$r_{OC} = [0,\ 0,\ 0.384\text{m}]$
Length to rolling bearing	$r_{OB} = [r_r\cos(\alpha),\ r_r\sin(\alpha),\ 0.211\text{m}]$
Shaft diameter	$d_r = 25$ mm
Parameter of the rolling bearing	
Inner diameter	$d_1 = 2r_1 = 28$ mm
Inner race outer diameter	$d_2 = 2r_2 = 37$ mm
Sphere radius	$r_{sph} = 5.0$ mm
Impact stiffness	$k_n = 2.5 \cdot 10^{10}$ N/m$^{3/2}$
Friction coefficient	$\mu = 0.20$
Restituition coefficient	$e = 0.90$
Parameter of the inner and outer house	
Mass from inner house	$m_{ih} = 1.70$ kg
Damping 1	$c_h = 7.04 \cdot 10^2$ Ns/m
Mass from outer housing	$M_{oh} = 8.87$ kg
Damping	$c_v = 2.28 \cdot 10^2$ Ns/m

3.2. Simulated results and experimental comparison.

As mentioned before, the test rig is a rotor suspended at one end by a removable passive bearing. From the moment that the magnetic force is removed, there are three distinct stages: a) the rotor free fall inside the bearing; b) contact

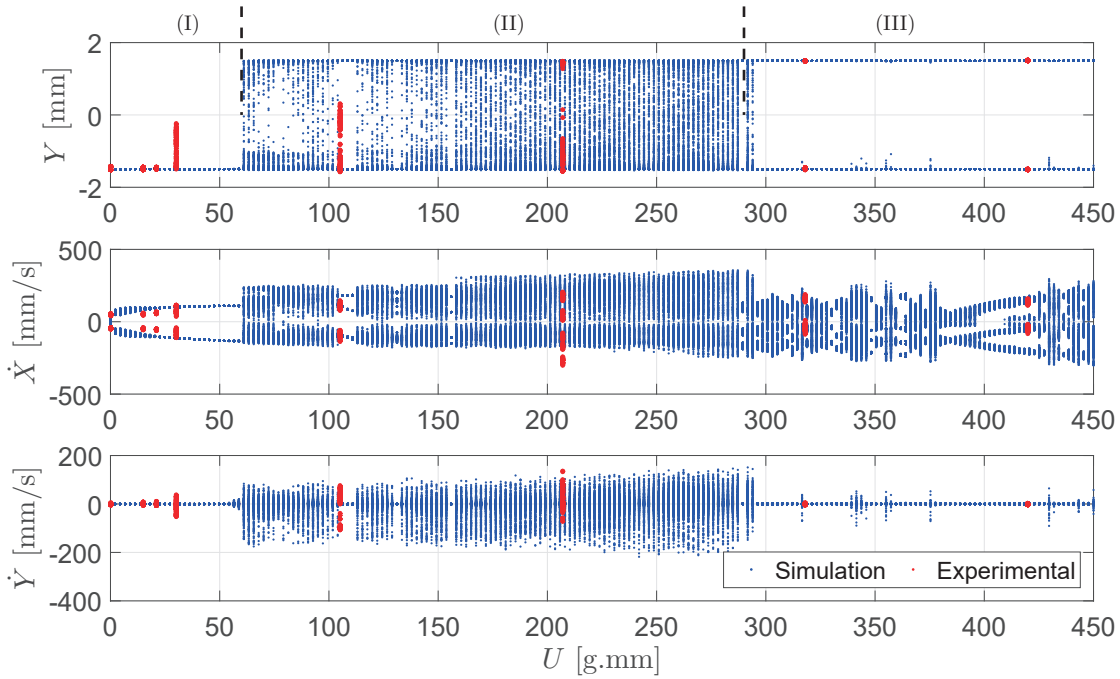

Fig. 4 10 Hz simulated bifurcation for different unbalance levels together with 8 different experimental tests with unbalance levels of: $U_1 = 0.0$ g.mm, $U_2 = 15$ g.mm, $U_3 = 21$ g.mm, $U_4 = 30$ g.mm, $U_5 = 105$ g.mm, $U_6 = 207$ g.mm, $U_7 = 318$ g.mm and $U_8 = 420$ g.mm.

between rotor and inner ring surfaces occurs leading to the deformation of the compliant and surface and angular acceleration of the inner race; and finally c) the relative velocities between the inner race and shaft surfaces almost vanish and the rotor fins a steady state condition at the bottom of the backup bearing. In fact, since the rotor keeps executing small translational movement around the equilibrium and rarely the relative velocity will coincide.Though this steady-state general dynamic behavior of the rotor changes significantly according to the unbalance level. After removing the magnetic force, the rotor falls and impacts several times on the surface of the inner race. The energy will be dissipated by the damping from the coupling between the inner and outer housing and from the impact with the compliant surface.

The changes in the steady-state behavior can be evaluated more explicitly with a Poincaré Map, Figure 4. The variables Y, $\dot{X}$ and $\dot{Y}$ are sampled every time the center of the shaft crosses the vertical line, in other words, when $X = 0$. The first plot on the top of Figure 4 shows the vertical position, Y, through which the rotor crosses the vertical line as a function of the control variable i.e. the unbalance, U.

Overall the phenomena are captured by both experiments and simulation. We can divide the bifurcation diagram into three specific regions. First the rotor center is always crossing at the bottom of the shaft at $Y = -1.5$ mm in region (I). Suddenly there is a change and more crossings at the vertical line occur. This can be seen in the region (II) of figure 4. The more unbalance the more evident that the center of the shaft performs chaotic trajectories. In the simulation it is expected to see the rotor crossing from the bottom to the top of the bearing, but the mechanical set up shows a gradual increase in the vertical crossing as the unbalance gets bigger until the rotor is able to perform a full whirl. In the right end of the plot, region III, the rotor is only executing a full whirl so the rotor is crossing the vertical line in the extremes, $Y = -1.5$ to $Y = 1.5$ mm. In the following plots, the horizontal and the vertical crossing velocity, $\dot{X}$ and $\dot{Y}$, are plotted against the unbalance and, once again, the experimental and the simulation tend to agree to each other.

To visualize the existence of chaotic trajectories performed by the rotor center, a double-sided spectrum is displayed in Figure 5a and b. Two levels of unblance are chosen: $U = 207$ g.mm from region (II) and $U = 420$ g.mm from region (III). The noise is significantly raised and several other peaks appear. This is a clear indication that chaos is happening. Higher unbalance levels show clearly higher peaks at $\Omega = -10.0$ Hz than its opposite pair, confirming the predominance of a full whirl at the same directions of the rotor spinning. Negative values of ω means the same spinning direction of the rotor.

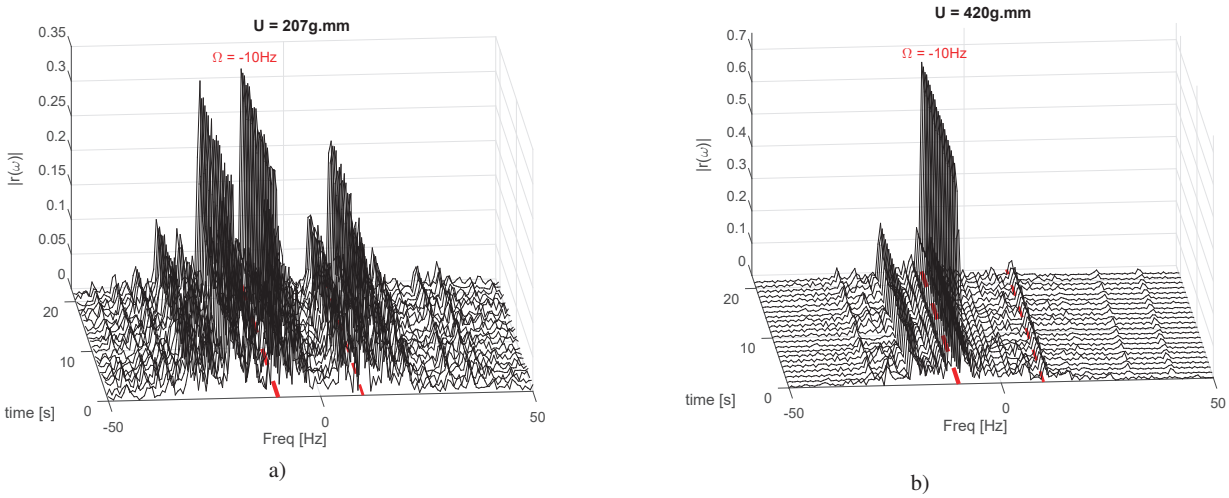

Fig. 5 Experimental 10 Hz double sided spectrum of the radial displacement, the unbalance corresponding to 0.27 kg.mm a) belongs to region II. For the unbalance corresponding to 0.42kg.mm b) A clear dominance of one peak at $\Omega = -10$ Hz indicates the full whirl in the same direction the shaft rotates stays in the region III.

4. Conclusion and Future Aspects

From the theoretical and experimental nonlinear analysis carried out in the paper, one can conclude that the rotor -backup bearing system has three distinguished dynamical behaviors depended on the level of rotor unbalance. Zone (I), characterized by low unbalance level from (0, 60] g.mm, simple oscillatory movementes of the rotor center at the bottom of the backup bearing are see. Zone (II) by unbalance levels from (60 to 280] g.mm, chaotic motions followed by impacts between rotor and backup inner race surface. Finally, zone (III) characterized by high unbalance levels, full forward whirl of the rotor center takes place.

There is much more to explore in this problem. The magnitude of the forces at the three different zones changes and supports the idea that it may damage the backup bearing. The relationship between the radii of the rotor and the inner race may also affect the magnitude of the forces and should be investigated in the next future. Different material properties and angular velocities shall contribute a lot to the response of the system and further results shall point in that direction.

5. Acknowledgement

The authors express their acknowledgement to CNPq through the Science Without Borders Program with the process number: 249728/2013-3, which sponsored the elaboration of this paper.

References

H. F. Black. Interaction of a whirling rotor with a vibrating stator across a clearance annulus. *Arch. J. Mech. Eng. Sci. 1959-1982 (vols 1-23)*, 10(1):1–12, 1968. ISSN 0022-2542. doi: 10.1243/JMES_JOUR_1968_010_003_02.

F. K. Choy and J. Padovan. Non-linear transient analysis of rotor-casing rub events. *Journal of Sound and Vibration*, 113: 529–545, 1987.

M. T. Cole, P. S. Keogh, and C. R. Burrows. The dynamic behavior of a rolling element auxiliary bearing following rotor impact. *ASME. J. Tribol.*, 2(124):406–413, 2001.

C. A. L. L. Fonseca, H.I. Weber, P.F. Fleischer, and I.F. Santos. Analyzing the use of pins in safety bearings. *J. Braz. Soc. Mech. Sci. Eng.*, 37:1425–1434, 2015.

M. A. Fumagalli. *Modelling and measurement analysis of the contact interaction between a high speed rotor and its stator*. PhD thesis, ETH - Swiss Institute Of Technology Zurich, 1997.

R. Gasch, R. Nordmann, and H. Pfützner. *Rotordynamik*. Springer Verlag, Berlin, 2nd ed., edition, 2002.

L. Ginzinger, B. Heckmann, and H. Ulbrich. Feedback control to prevent damage by rotor rubbing after an impact load. *Proceedings of the Asme Turbo Expo, Proc. Asme Turbo Expo*, 6:1003–1012, 2009. doi: 10.1115/GT2009-60195.

P. Goldman and A. Muszynska. Chaotic Behavior of Rotor/Stator Systems With Rubs. *J. Eng. Gas Turbines Power*, 116 (3):692, 1994.

J. I. Inayat-Hussain. Nonlinear dynamics of a magnetically supported rigid rotor in auxiliary bearings. *Mechanism and Machine Theory*, 45(11):1651–1667, 2010.

J. Jiang and H. Ulbrich. The Physical Reason and the Analytical Condition for the Onset of Dry Whip in Rotor-to-Stator Contact Systems. *J. Vib. Acoust.*, 127(6):594, 2005. ISSN 07393717. doi: 10.1115/1.1888592.

D. C. Johnson. Synchronous whirl of a vertical shaft having clearance in one bearing. *Arch. J. Mech. Eng. Sci. 1959-1982 (vols 1-23)*, 4(1):85–93, 1962. ISSN 0022-2542. doi: 10.1243/JMES_JOUR_1962_004_012_02.

P. S. Keogh. Contact dynamic phenomena in rotating machines: Active/passive considerations. *Mech. Syst. Signal Process.*, 29:19–33, may 2012. ISSN 08883270. doi: 10.1016/j.ymssp.2011.06.024.

R. G. Kirk. Transient Response Technique Applied to Active Magnetic Bearing Machinery During Rotor Drop. *Transactions of the ASME*, 118(April 1996), 1996.

S. Lahriri and I. F. Santos. Experimental quantification of dynamic forces and shaft motion in two different types of backup bearings under several contact conditions. *Journal Mechanical Systems and Signal Processing*, 2012.

H. M. Lankarani and P. E. Nikravesh. A Contact Force Model With Hysteresis Damping for Impact Analysis of Multibody Systems. *J. Mech. Des.*, 112(3):369, 1990.

A. Muszynska. Rotor-to-stationary element rub-related vibration phenomena in rotating machinery - literature survey. *Shock and Vibration Digest*, 21(3):3–11, 1989. ISSN 05831024, 17413184.

H. C. Piccoli and H. I. Weber. Experimental observation of chaotic motion in a rotor with rubbing. *Nonlinear Dyn.*, 16 (1):55–70, 1998.

J. C. Pradetto and J. Schmied. Behaviour of a one ton rotor being dropped into auxiliary bearings. In *Proceeding 3rd Int. Symp. Magn. Bear.*, pages 145–156, 1992.

G. Schweitzer. Stabilization of self-excited rotor vibrations by an active damper. *Dynamics of rotors*, pages 472–493, 1975.

G. Schweitzer and E. H. Maslen. *Magnetic Bearings*. Springer-Verlag Berlin Heidelberg, 1 edition, 2009.

U. Simon. *Rotor Stator Kontakt in polygonförmigen Fanglagern*. PhD thesis, Technischen Universität CaroloWilhelmina zu Braunschweig, 2001.

X. X. Wang and S. S. Noah. Nonlinear dynamics of a magnetically supported rotor on safety auxiliary bearings. *ASME. J. Vib. Acoust.*, 2(120):596–606, 1998.

Wojciech, M. S. *Dynamisches Verhalten eines schnell drehenden Rotors bei Anstreifvorgangen*. PhD thesis, TU Karlsruhe, 1986.

W Zhang. Dynamic instability of multi-degree-of-freedom flexible rotor systems due to full annular rub. *IMechE C252/88*, pages 305–308, 1988.

D. Zülow and R. Liebich. Ein aussenrollenlager als fanglagerkonzept für magnetgelagerte rotoren. In *SIRM 8. Internationale Tagung Schwingungen in rotierenden Maschinen, Wien, Austria, paper-ID 11*, 2009.